

Hydrodynamic Analysis of the Spherical Underwater Robot SUR-II

Regular Paper

Chunfeng Yue¹, Shuxiang Guo^{2,3,*} and Liwei Shi^{2,*}

1 Graduate School of Engineering, Kagawa University, Takamatsu, Japan

2. Faculty of Engineering, Kagawa University, Takamatsu, Japan

3. School of Electrical Engineering, Tianjin University of Technology, Tianjin, China

* Corresponding author E-mail: s12d502@stmail.eng.kagawa-u.ac.jp

Received 3 Jul 2012; Accepted 9 Apr 2013

DOI: 10.5772/56524

© 2013 Yue et al.; licensee InTech. This is an open access article distributed under the terms of the Creative Commons Attribution License (<http://creativecommons.org/licenses/by/3.0>), which permits unrestricted use, distribution, and reproduction in any medium, provided the original work is properly cited.

Abstract This paper describes the development of the second-generation Spherical Underwater Robot (SUR-II). The new SUR-II has an improved propulsion system structure, resulting in better performance compared with the original design. This paper focuses on the characteristics of the water-jet thruster and the spherical hull of the SUR-II. To analyse its hydrodynamic characteristics, the main hydrodynamic parameters of the SUR-II were estimated based on two reasonable assumptions and a reasonable dynamic equation was proposed to describe the relationship between force and velocity. Drag coefficients were calculated separately for vertical and horizontal motions due to the fin on the robot's equator and the holes in the robot's hull. The holes had a particularly adverse effect on the horizontal drag coefficient. A hydrodynamic analysis using computational fluid dynamics was then carried out to verify the estimated parameters. The velocity vectors, pressure contours and drag coefficient for each state of motion were obtained. Finally, the propulsive force was determined experimentally to verify the theoretical calculations and simulation results.

Keywords Spherical Underwater Robot, Hydrodynamic Analysis, Hydrodynamic Characteristics Estimation

1. Introduction

The applications of autonomous underwater vehicles (AUVs) have been expanding and now include fields such as ocean research, scientific investigations, ocean development and underwater projects. The development of autonomous underwater vehicles has reached a level of practical technological maturity. Autonomous underwater vehicles can be divided into two categories based on whether or not their bodies are streamlined. The vehicle's shape is determined by the requirements of the application. For example, a streamlined shape reduces water resistance and is preferable if the vehicle must move at high speeds. However, if underwater detection or operation tasks are the primary roles of an underwater robot, a non-streamlined shape is often used.

Different tasks require autonomous underwater robots to be of different shapes and sizes. Deep-sea research requires high water-pressure resistance, while monitoring and observation tasks require small, flexible and stable robots. Research in fields such as hydrodynamics, electronics and mechanics is necessary in order to build a robot with good motion-control performance. The research is often interdisciplinary; for example,

mechanics and hydrodynamics are both used in designing mechanical structures that will provide optimal hydrodynamic characteristics.

Due to the good water-pressure resistance of spherical objects, spherical robots can perform a rotational motion with a 0° turn radius. Many types of spherical underwater robots have been developed. ODIN-III was a typical prototype robot developed at the University of Hawaii [1, 2]. It had a metal shell, a diameter of 630 mm and a weight of 150 kg. This spherical underwater robot was used to monitor the environment and for underwater operations. Researchers at the University of Manchester and Oxford University co-developed a micro-spherical underwater robot [3, 4]. This robot used six propellers in its propulsion system located around the equator of its spherical hull. This micro-robot was developed to monitor nuclear storage ponds and wastewater treatment facilities to prevent leakage. Both of these robots used propellers on the outside of their bodies for their propulsion systems. Other spherical underwater robots have used water-jet thrusters. Researchers at Harbin Engineering University developed a spherical underwater robot with three water-jet thrusters [5, 6]. However, the propulsive force of the thrusters was considerably reduced because the water input pipeline was curved. Researchers at the Beijing University of Post and Telecommunications developed a spherical underwater robot with one tunnel propeller [7]. This robot adjusted its attitude by changing its centre of mass by using a movable weight-balancing block. This made it possible to adjust the direction of the tunnel propeller and to achieve some linear motion, but the robot could not carry out other hybrid motions because it only had one propeller.

In our laboratory, we developed a spherical underwater robot that used three vectored water-jet thrusters for its propulsion system [8–11]. The propulsion system was assembled inside the spherical hull to reduce its effects on the robot's flexibility and to limit damage from possible impacts.

1.1 Related Work

Hydrodynamic characteristics are important factors in research into underwater vehicles. The efficiency and accuracy of the control algorithms and the optimum structure of the robot depend on hydrodynamic analyses; so many researchers have carried out hydrodynamic analyses on their underwater vehicles. Ueno *et al.* analysed the Submersible Surface Ship (SSS), a new type of ship that can avoid rough seas by going underwater using the downward lift of wings while maintaining residual buoyancy for safety [12]. They set up a tank experiment to analyse its hydrodynamic characteristics and then proposed a mathematical model to describe the

interaction effects based on the resulting data. Leroyer *et al.* analysed the DTMB5415 bare hull using a computational fluid mechanics (CFD) method and proposed two numerical procedures that sped up the Reynolds-averaged Navier–Stokes (RANS) solvers [13]. They were able to obtain numerical solutions to realistic problems up to four times faster using these two procedures. Mylonas and Sayer predicted the forces acting on a yacht keel based on large-eddy simulation (LES) and detached-eddy simulation (DES) solutions [14]. Propulsion systems have also been a main research subject. Wei *et al.* predicted the propeller-excited acoustic response of a submarine structure using a numerical method [15]. Cheng *et al.* analysed the hydrodynamic characteristics of an unconventional propeller with an end-plate effect and compared the results to those of a conventional propeller [16]. Ji *et al.* verified that acceleration due to changes in cavity volume is the main source of the pressure fluctuations excited by propeller cavitation [17]. All of these studies involved propellers and researchers have used many different methods to analyse various hydrodynamic characteristics.

1.2 Motivation

The Spherical Underwater Robot (SUR) has a unique hull and a unique propulsion system. Therefore, hydrodynamic analysis is an important requirement for the motion control system of the robot. We conducted hydrodynamic analyses to obtain the main hydrodynamic parameters of the robot, which reflect its performance. Water resistance and pressure distribution are important features when investigating interactions between a robot and fluid, and the drag coefficient is an important parameter when analysing the force of water drag.

The hydrodynamic characteristics of an underwater robot differ for each motion. In previous work, we assumed that the robot was a sphere, so the motion features were the same for all degrees of freedom. However, our previous analyses did not yield sufficiently accurate results, because water flows through the holes in the robot's hull during horizontal motion and the motion of fluid is affected by the fin around the robot's equator. Also, the propulsive force influences the flexibility of the robot; therefore, we analysed the propulsive force based on simulated and theoretical calculations.

1.3 Paper Outline

This paper is structured as follows. Section 1 provides background for the research. Section 2 describes the second-generation Spherical Underwater Robot (SUR-II), which has an improved water-jet propulsion system. This section also provides the motion states of the robot to each degree of freedom. Section 3 presents the main

hydrodynamic parameters of the SUR-II and analyses its motions in detail. Section 4 presents a hydrodynamic analysis based on CFD. Section 5 describes an experiment used to verify the propulsive force analysis and Section 6 summarizes our conclusions.

2. Mechanical Structure Analysis

We have already conducted extensive research on the SUR and obtained some useful results. Lin designed the first-generation SUR and implemented its basic motion control [18, 19].

2.1 Analysis of the Vectored Water-jet Thruster

The static analysis is very important for this robot. First, unexpected deformation occurs in the propulsion system. The deformation of the propulsion system of the first-generation robot has some negative effects [18, 19]. With the vectored water-jet thruster, we control the direction of the thruster in order to implement some underwater motions. However, the deformation will affect the direction of the nozzle. As a result, the direction of the propulsive force cannot be controlled very accurately. In addition, if the propulsion system is not rigid enough, vibrations will also be caused very easily. Second, the weight of the robot is to be reduced to increase the robot's payload capacity. Therefore, a static analysis of the propulsion system was carried out to improve its mechanical features. A Newton propulsive force acts on each nozzle of the water-jet thruster. The thruster operates in three orientations: up, down, and horizontal; therefore, the static analysis was divided into three states. When the frame and triangular support of the propulsion system was improved, as shown in Figure 1, it reduces the deformation of the vectored water-jet thruster and reduces the weight of the propulsion system to 1.08kg.

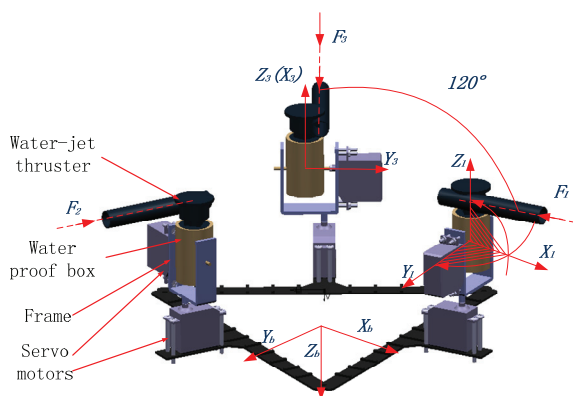
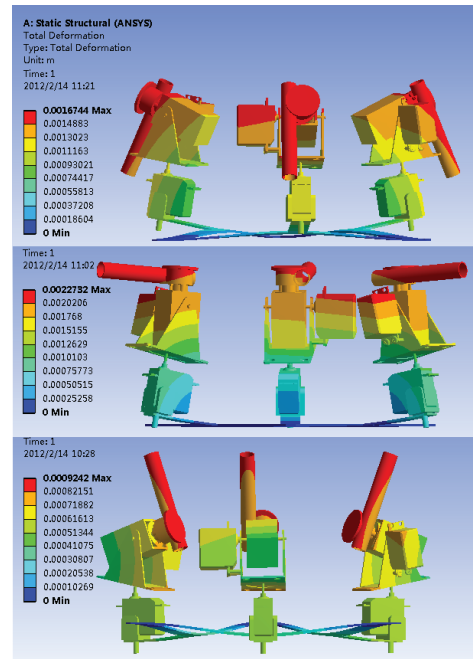


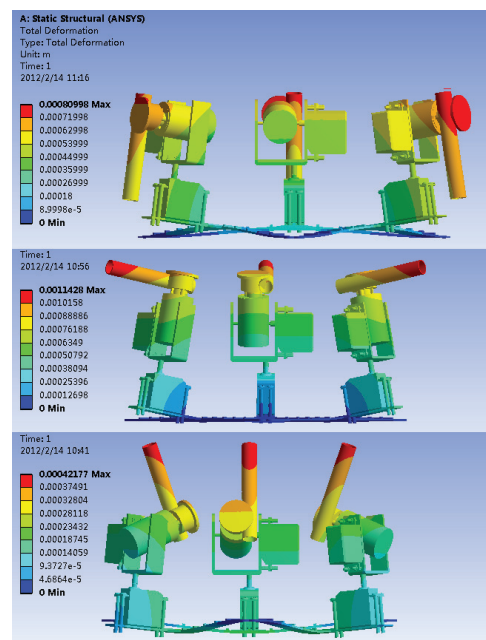
Figure 1. Structure of the vectored water-jet thruster after improvement

The static analysis results of the improved propulsion system, shown in Figure 2 (b) [20], indicate that the largest deformation was about 2 mm before the improvement and the deformation will cause an angle

error of about 1.5 degrees. After the improvement, the deformation is reduced to 1mm and the angular error is reduced to 0.7 degrees. Therefore, the direction of the propulsive force of the propulsion system is more accurate. The second-generation Spherical Underwater Robot (SUR-II) contains the improved vectored water-jet thruster.



(a) previous design



(b) improved

Figure 2. Deformation of the propulsion system after improvement

The vectored water-jet thruster is composed mainly of four components: one water-jet thruster, one waterproof box, two servomotors and one support frame. The water-

jet thruster provides the propulsive force for the SUR-II. The servomotors are employed to change the direction of the water-jet thruster. The waterproof box protects the DC motor of the water-jet thruster from water. The support frame is a basic component of the water-jet thruster.

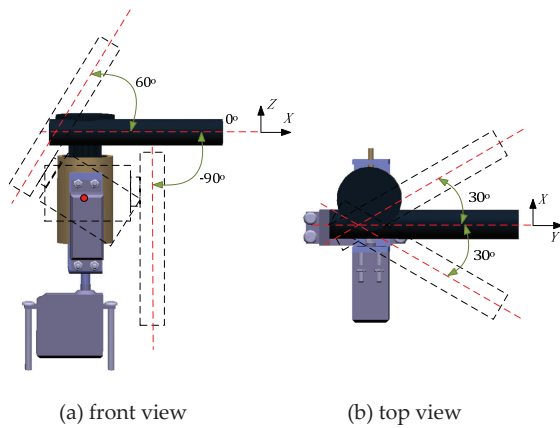


Figure 3. Range of rotation in the horizontal and vertical planes

Each vectored water-jet thruster has two rotational degrees of freedom. Figure 3(a) shows the range of rotation from -90 to $+60$ degrees in the vertical direction. Vertical motion of the SUR-II is possible due to the rotational degree of freedom in the vertical direction. Figure 3(b) shows that the range of rotation is 60° in the horizontal direction. The servomotors not only adjust the thruster orientation, but also generate resistance torque to ensure that the thruster orientation remains in the correct position.

2.2 Analysis of the SUR-II Structure

Figure 4 shows the conceptual design of the SUR-II. The waterproof box contains all of the control circuits and several sensors. The robot can be divided into four systems: the propulsion system, control system, sensor system and mechanical system.

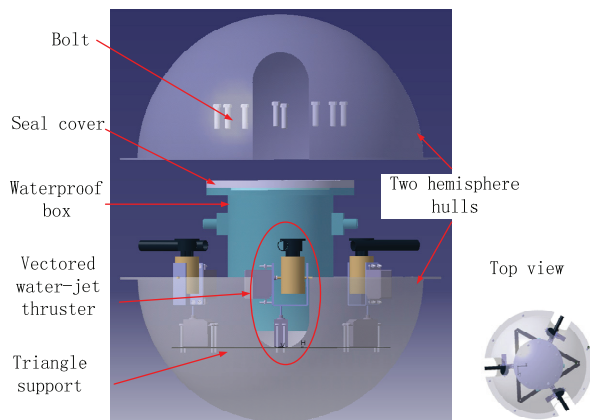


Figure 4. Conceptual design of the SUR-II

For the propulsion system, three vectored water-jet thrusters are assembled on a triangular support. The

system is installed inside the hull for two reasons. First, underwater environments are complex and a variety of creatures live in the water. Having the propulsion system installed in the hull can effectively prevent external impacts. Second, the hull of the robot can then be designed to approximate a sphere and the influence of the propulsion system on the hydrodynamic characteristics of the robot would be reduced in compared with if it were installed outside the hull.

DOF	Surge	Sway	Heave	Roll	Pitch	Yaw
Utilization ratio	100%	31%	96%	33%	7%	100%

Table 1. The utilization ratio of each degree of freedom for underwater vehicles

Generally, an underwater vehicle has six degrees of freedom, but not all of these can be used for actual movements. Table 1 shows the typical utilization ratio of each degree of freedom in an underwater vehicle [21]: sway, pitch and roll are seldom used. The SUR-II has four degrees of freedom: surge, sway, heave and yaw. Because the SUR-II is symmetric in its geometric centre and has a 0° turn radius, sway has thus far not been employed. Therefore, only three degrees of freedom must be considered in detail: surge, heave, and yaw.

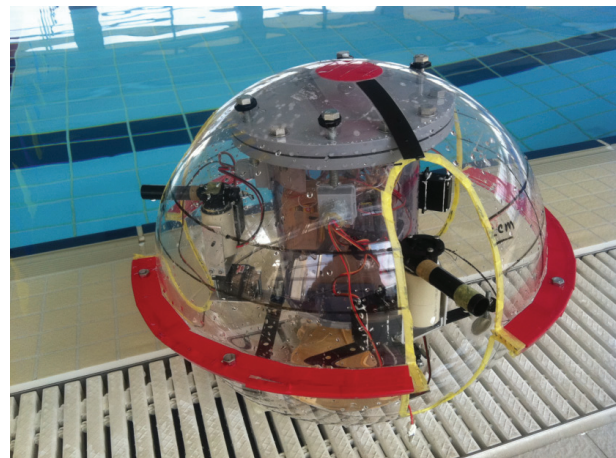
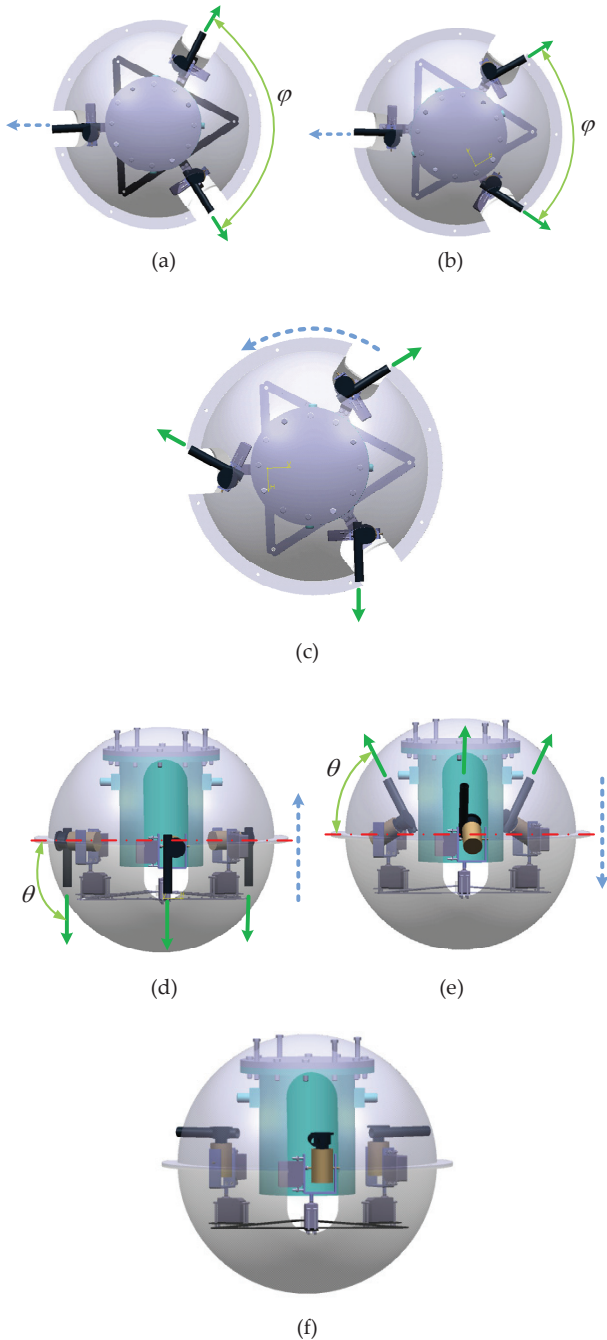


Figure 5. Spherical underwater robot

2.3 Motion States of the SUR-II

The three main degrees of freedom were analysed in detail: surge, heave, and yaw. In general, two water-jet thrusters are employed to provide propulsive force for surge motion and the third can be used as a brake. If high speeds are required, the angle of the propulsive force can be adjusted by horizontal servomotors, as shown in detail in Figures 6(a) and (b). Rotational motion is shown in Figure 6(c); the rotational angle can be measured by using the feedback from a gyroscope. Figures 6(d), (e), and (f) present the up, down and hold positions, respectively.



---▶: the direction of motion; →: the direction of the propulsive force.

Figure 6. Basic motion states; (a) is regular motion in surge; (b) is quick motion in surge; (c) is rotation in yaw; (d), (e), (f) are vertical motion in heave.

3. Dynamic Analysis

Hydrodynamic characteristics play a direct role in hydrodynamic analysis, which can be used to verify the accuracy of the estimation of the main hydrodynamic parameters. The estimation of the parameters was based on the following assumptions:

1. The robot is a sphere;
2. The fluid environment is static water at 20°C.

3.1 Dynamic Model of the SUR-II

Considering all of the factors that influence the SUR-II, a six-dimensional dynamic equation was established:

$$(M_{RB} + M_{add})\dot{v} + (D_l + D_q(v))v + (C_{RB}(v) + C_A(v))v + g(\Theta) = \tau \quad (1)$$

where M_{RB} denotes the rigid body mass matrix, M_{add} is the added mass of the spherical underwater robot, $C_{RB}(v)$ is the rigid body Coriolis matrix, $C_A(v)$ is the hydrodynamic Coriolis matrix, $D_l v$ is the linear damping term, $D_q(v)v$ is the nonlinear damping term, $g(\Theta)$ is the restoring force vector and τ is the control vector, which contains the propulsive force and the moment. The following simplifications can be proposed based on the discussion in Section 2. First, the roll and pitch movements are passively controlled, so they are negligible. Second, the surge and sway movements have the same dynamic features due to the spherical shape. Therefore, the dimensions of Equation 1 can be reduced to three. Coriolis forces are caused by the earth's rotation and the speed of the moving object. The speed of the SUR-II robot is less than 0.3 m/s, and most of the factors in the Coriolis matrix are related to the robot's velocity, so Coriolis forces can be ignored for these low-speed cases. In hydrodynamics terminology, gravitational and buoyancy forces are called restoring forces, $g(\Theta)$. The buoyancy forces are almost solely determined by the waterproof box. The position of water proof box can be adjusted using 4 long screws. Hence, the centre of buoyancy is adjustable. In real situations, the restoring force exists. However, it has no influence on the motion of surge, sway, heave and yaw. Its only effect in this case is to adjust the rotation motion of pitch and roll which were not considered in this paper and, as such, we ignored the $g(\Theta)$. Therefore, Equation 1 becomes:

$$(M_{RB} + M_{add})\dot{v} + (D_l + D_q(v))v = \tau \quad (2)$$

where τ is measurable using a propulsive force experiment. The parameters of Equation 2 must be determined accurately to enhance the accuracy of the dynamic analysis.

3.2 Related Parameter Estimation

M_{add} is calculated based on the spherical shape:

$$M_{add} = \frac{2}{3} \rho \pi R^3 \quad (3)$$

M_{RB} can be obtained with measurements and the use of a 3D model:

$$M_{RB} = \begin{bmatrix} m & 0 & 0 \\ 0 & m & 0 \\ 0 & 0 & I_{zz} \end{bmatrix} = \begin{bmatrix} 6.3 & 0 & 0 \\ 0 & 6.3 & 0 \\ 0 & 0 & 0.1281 \end{bmatrix},$$

$$M_{\text{add}} = \begin{bmatrix} 16.75 & 0 & 0 \\ 0 & 16.75 & 0 \\ 0 & 0 & 0.3864 \end{bmatrix}$$

Based on Assumption 2 and Equation 4, $D\dot{v} = C_l \times \text{diag}\{u, v, w, p, q, r\}$, where $C_l = 1 \times 10^{-4}$ is the linear viscous coefficient of the fluid at 20°C, and $\text{diag}\{u, v, w, p, q, r\}$ is the velocity matrix of the robot. Because the velocity is very small, $D\dot{v}$ can also be neglected. This simplifies Equation 2 to:

$$(M_{\text{RB}} + M_{\text{add}})\dot{v} + F_d = \tau \quad (4)$$

F_d can be calculated as:

$$D_q(v)v = F_d = \frac{1}{2} C_d (R_e) \rho V^2 A \quad (5)$$

where C_d is the drag coefficient, R_e is the Reynolds number, which reflects the flow characteristics, V is the velocity vector and A is the cross-sectional area.

When the robot moves in vertically, the ring fin that is fixed on the spherical hull equator cannot be ignored. The ring width is $r = 30$ mm, so $A' = \pi (R + r)^2 = 0.1662$ m². When the robot moves horizontally, the fin can be ignored, so $A = \pi R^2 = 0.1256$ m², where $R = 200$ mm is the radius of the robot.

For a spherical shape, C_d is determined by R_e : [22]

$$R_e = \frac{vD}{\nu} \quad (6)$$

where ν is the kinematic viscosity of the fluid, and $\nu = 1 \times 10^{-6}$ at 20°C. The maximum velocity is 0.3 m/s, so $R_e = 1.2 \times 10^5 > 1 \times 10^3$, which indicates that the flow is turbulent when the robot moves through the water. Based on Table 2, when $R_e = 1.2 \times 10^5$, $C_d = 0.40$. For vertical motion, $F_{Hd} = c^2 v^2$, where $c^2 = 33.24$. The propulsive force is equal to F_d . When the robot moves at maximum velocity, $F_d = T$, where T can be obtained experimentally. The result $T = 2$ N will be verified in Section 5.

R_e	$R_e < 10^4$	$10^4 < R_e < 3 \times 10^5$	$3 \times 10^5 < R_e < 1 \times 10^6$
C_d	$24/R_e + 6.48 \times R_e^{-0.573} + 0.36$	0.40	0.40
C_d	$30/R_e + 0.46$	0.46	0.46
C_d	$24/R_e + (1 + 0.0654 R_e^{2/3})^{3/2}$	0.40	0.40
C_d	$(0.352 + (0.124 + 24/R_e^{1/2})^2)$	-	-
C_d	$(0.63 + 4.8 \times R_e^{-0.5})^2$	0.40	-

Table 2. [23,24] Relationship between R_e and C_d for a spherical shape

For vertical motion, C_d cannot be obtained from Table 2 because the holes influence the hydrodynamic characteristics. Fluid flows through the holes, so the robot cannot be classified as closed. However, at high speeds

the maximum velocity $v_{\text{max}} = 0.3$ m/s and propulsive force $T = 2\sqrt{3}$ N. Based on Equation 5, $C_d = 0.5 \rho v^2 A / T = 0.61$. After comparing the two values of the drag coefficient, we found that the holes in the spherical hull increased water resistance.

For the robot's rotational motion, the nonlinear damping term is zero because the robot has a symmetrical shape.

After analysing and calculating the parameters of the dynamic equation, we obtained:

$$\begin{bmatrix} 23.05 & 0 & 0 \\ 0 & 23.05 & 0 \\ 0 & 0 & 0.5145 \end{bmatrix} \dot{v} + \begin{bmatrix} 39.25v & 0 & 0 \\ 0 & 33.24v & 0 \\ 0 & 0 & 0 \end{bmatrix} v = \begin{bmatrix} 2T \cos \frac{\phi}{2} \\ T \sin \theta \\ M_z \end{bmatrix} \quad (7)$$

where ϕ is the angle of the two working thrusters for horizontal motion and θ is the angle of the thruster for vertical motion. The relationship curves that describe how velocity varies with time were obtained using Equation 7, based on the motion shown in Figure 6 and $\phi = 2\pi/3, \pi/3$. The results are presented in Figures 7 and 8. Table 3 demonstrates that the maximum speed in each direction of motion is different, based on the results of Figures 7 and 8, and shows that the acceleration time is less than 10 seconds.

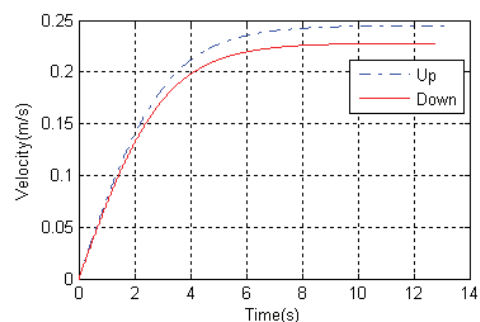


Figure 7. Variation of speed with heave in time

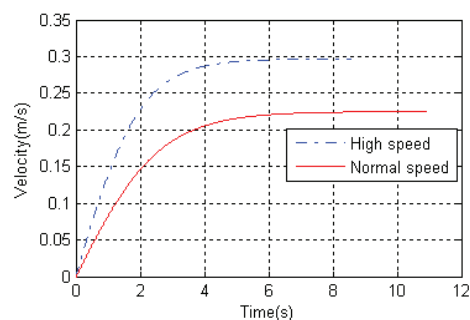


Figure 8. The curves that show that speed varies with time in surge

Motion state	Heave		Surge	
	Up	Down	Normal speed	High speed
V_{max} (m/s)	0.245	0.228	0.225	0.3
Time consumption(s)	9	9	9	7

Table 3. Maximum velocity in heave and surge motion

4. Hydrodynamic Analysis

4.1 Hydrodynamic Analysis of the SUR-II

The SUR-II was modelled in a cylindrical flow field with a radius of 1 m and a length of 4 m, as shown in Figure 9. An unstructured tetrahedron mesh was adopted. The mesh density was increased around the robot and three boundary layers were used to obtain satisfactory results and reduce the amount of time required. Figure 9 presents the mesh for horizontal motion.

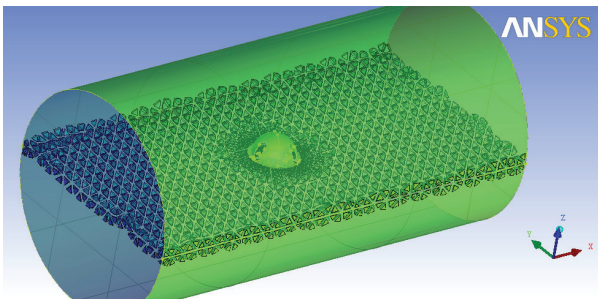


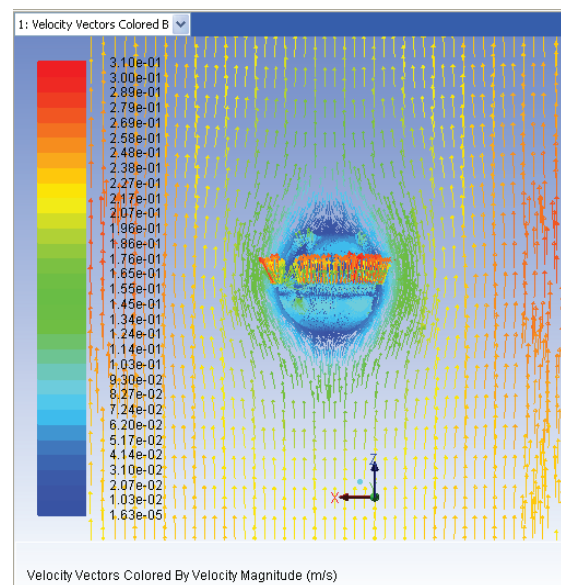
Figure 9. 3D model mesh

The quality of the mesh is a determining factor in the accuracy of hydrodynamic analysis. Therefore, the mesh was smoothed before carrying out the analysis and the 3D model was simplified before meshing. For example, nuts and bolts were ignored to reduce the complexity of the mesh and enhance the mesh quality. The various robot components were established as a single body. A total of 1.5 million mesh elements were used.

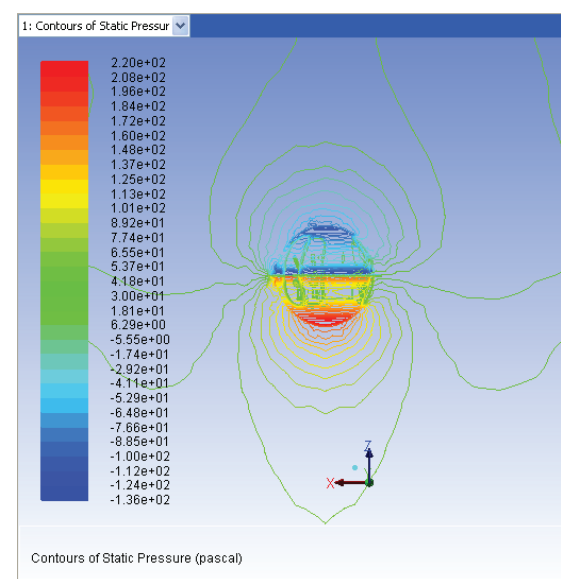
After completing the preliminary work, the mesh files were output to the solver. The commercial software package FLUID was employed to simulate the flow around the SUR-II. Three typical models were established: one for downward motion with a speed of 0.228 m/s, one for surge motion with a speed of 0.3 m/s and one for rotational motion with a speed of 3 rad/s. According to Table 3 and the Reynolds number criterion, turbulent flow occurred in all cases. Therefore, the main parameter settings for the hydrodynamic analysis were as follows: inlet: velocity inlet; outlet: outflow; viscous model: standard k-epsilon; convergence criterion: 0.0001.

The robot and fluid move relative to each other, so the robot was set as a static wall while the fluid was set as a constant velocity flow. Figures 10 and 11 present how both the velocity and pressure were affected by the fin that was fixed on the equator of the robot. Thus, the fin

cannot be ignored. However, the effect of the holes was not obvious. Figure 11 shows a cutaway view of the robot during vertical motion. The velocity of the fluid inside the robot was the same as the velocity of the robot. Therefore, the fluid inside the robot can be assumed as being part of the robot and Assumption 1 is valid. However, for horizontal motion (Figure 12), the simplifications are the opposite of those appropriate for vertical motion: the fin can be ignored and the holes must be considered, because water flows into the robot through the front holes and then out of the robot through the back holes, as shown in Figure 13. Thus, the robot cannot be assumed to be a closed sphere. In summary, the fins cannot be ignored for vertical motion and the holes cannot be ignored for horizontal motion.

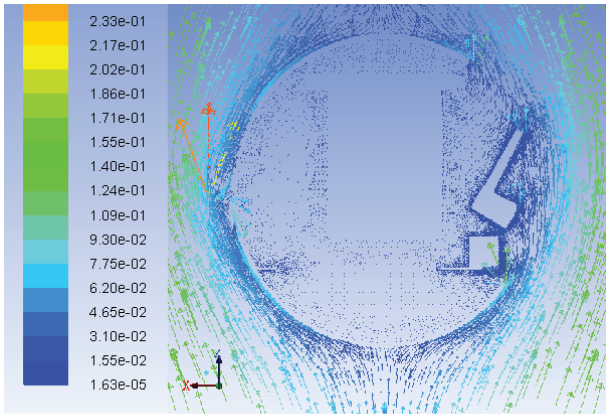


(a) Velocity vectors



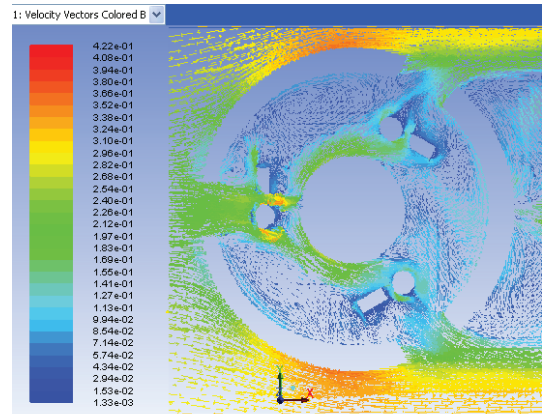
(b) Pressure contours

Figure 10. Influence of robot on the fluid during downward motion



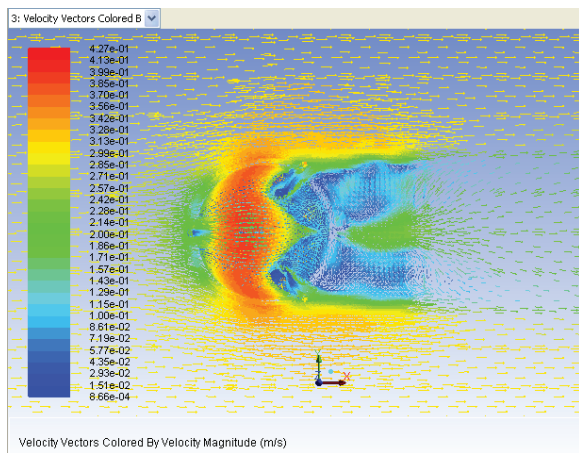
Velocity Vectors Colored By Velocity Magnitude (m/s)

Figure 11. Cutaway view of velocity vectors in vertical motion



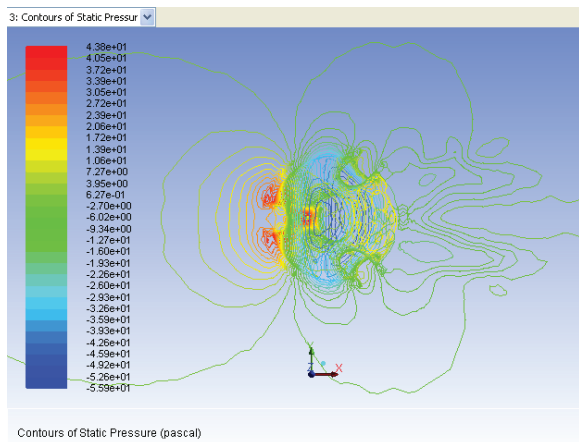
Velocity Vectors Colored By Velocity Magnitude (m/s)

Figure 13. Cutaway view of velocity vectors in horizontal motion



Velocity Vectors Colored By Velocity Magnitude (m/s)

(a) Velocity vectors

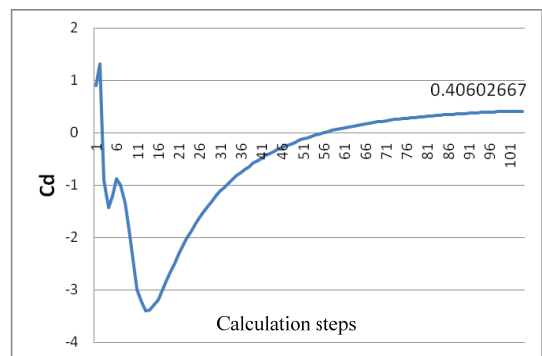


Contours of Static Pressure (pascal)

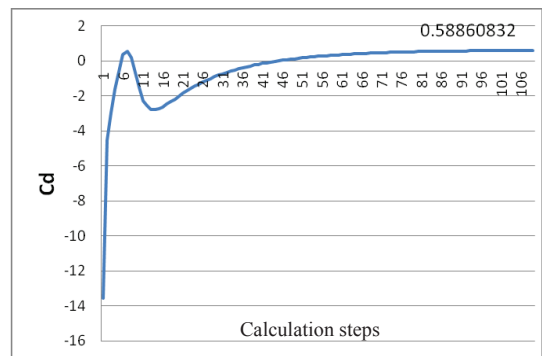
(b) Pressure contours

Figure 12. The influence of the robot on the fluid when the robot is moving horizontally

C_d was obtained from the simulations, as shown in Figure 14. After calculating about 100 steps, the drag coefficient for vertical motion converged to a constant $C_d = 0.40602667$, similar to the value calculated in Section 3. For horizontal motion $C_d = 0.58860832$, which indicates a 3% error compared to the calculated value. Therefore, the results of the CFD analysis are acceptable.



(a)

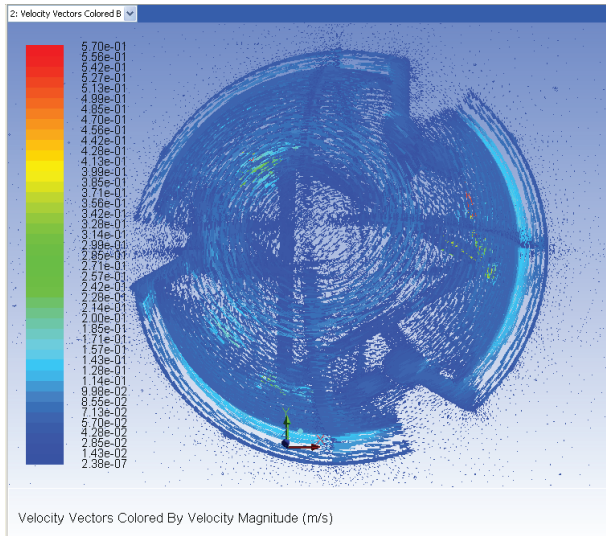


(b)

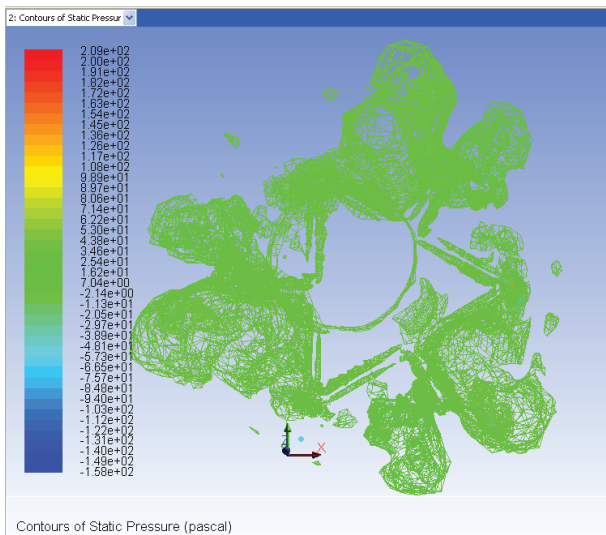
Figure 14. Drag coefficient: (a) vertical motion and (b) horizontal motion

After obtaining the drag coefficient, Equation 7 can be modified as follows:

$$\begin{bmatrix} 23.05 & 0 & 0 \\ 0 & 23.05 & 0 \\ 0 & 0 & 0.5145 \end{bmatrix} \dot{v} + \begin{bmatrix} 36.99v & 0 & 0 \\ 0 & 33.74v & 0 \\ 0 & 0 & 0 \end{bmatrix} v = \begin{bmatrix} 2T \cos \frac{\phi}{2} \\ T \sin \theta \\ M_z \end{bmatrix} \quad (8)$$



(a)



(b)

Figure 15. Yaw motion: (a) velocity vectors; (b) pressure contours

In addition to vertical and horizontal motion, rotational motion was also simulated. The velocity and pressure results indicated that the effect of rotational motion on the fluid was negligible. The interaction between the fluid and the robot was caused by the propulsion system, as shown in Figure 15, and a pressure surface was generated around the propulsion system.

4.2 Hydrodynamic Analysis of the Thruster

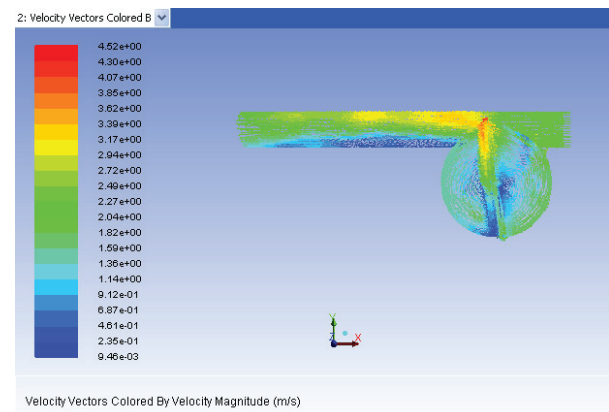
The water-jet thrust was also simulated to analyse the propulsive force and the propulsion system in detail. Figure 16(a) presents the robot thruster. Because the object of study was only a nozzle and blade, other parts were omitted in the 3D model, as shown in Figure 16(b).

In the simulation, the blade was set as the rotating part and the inlet was set as a velocity inlet. The maximum velocity occurred at the edge of the blade, as shown in

Figure 16(b). Due to the friction of the nozzle and the water resistance, the outlet velocity was about 2.5 m/s. Strong turbulence occurred in the nozzle. The propulsive force obtained by post processing was $T = 2.18446$.



(a)



(b)

Figure 16. Yaw motion: (a) water-jet thruster; (b) velocity vectors

We analysed both the robot and the thruster using separate hydrodynamic analyses. However, the two flow fields interact when the robot is moving, while the hydrodynamic analyses only focused on the basic motions. If a hybrid motion is also required, a dynamic mesh must be employed to describe the fluid field.

5. Experiment

5.1 propulsive force experiments

The propulsive force was determined experimentally to verify the theoretical and simulation results in Sections 3 and 4. In this experiment, a six degree-of-freedom load cell was employed to measure the propulsive force of the thruster. Figure 17 illustrates the principle of the experiment. When the thruster is working, the propulsive force acts on the nozzle. The difference of the moment acting on the XY plane is caused by the propulsive force and the arm of the propulsive force is measurable. Therefore, the propulsive force can be calculated; Figure 18 presents the results.

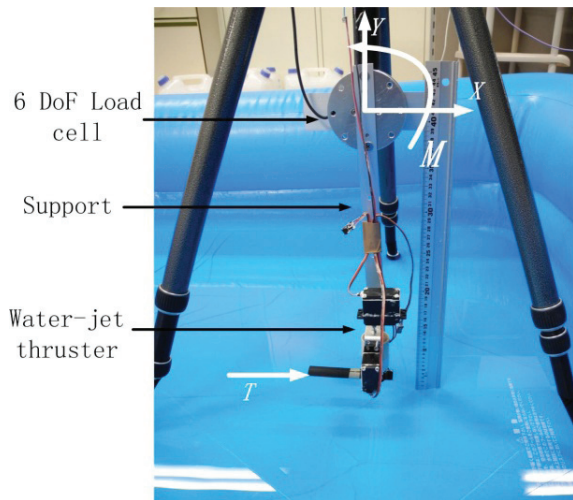


Figure 17. Principle of propulsive force experiment

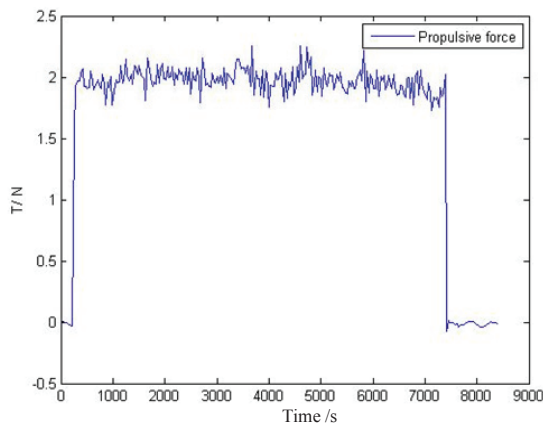


Figure 18. Propulsive force

In the experiment, the thruster operated for about 2 hours. Although the DC motor caused some vibrations, the mean value was 2 N.

5.2 Vertical motion experiment

To evaluate the improved propulsion system, we carried out a vertical motion experiment in a pool, which was also done using the previous robot SUR [8]. These two experiments were carried out in the same pool with the same control algorithm. The depth of the pool was 110 cm. First, the robot stayed in the initial position with a depth of 20 cm. Then it dived from 20 cm to 90 cm. Finally, the robot floated upward to 20 cm. In [8], we compared the experimental results with the simulation results and obtained the position errors of the vertical motion, as shown in Fig. 20 (a), of which the maximum error is about 15 cm. For the improved propulsion system, we also recorded the trajectory of the robot's geometrical centre during the diving/floating motion. Figure 20 (b) shows the experimental and simulation results of the improved robot, from which we can see that the position error for vertical motion is greatly reduced and the maximum error is about 10 cm.

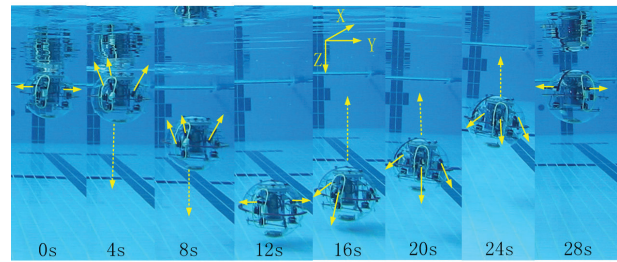
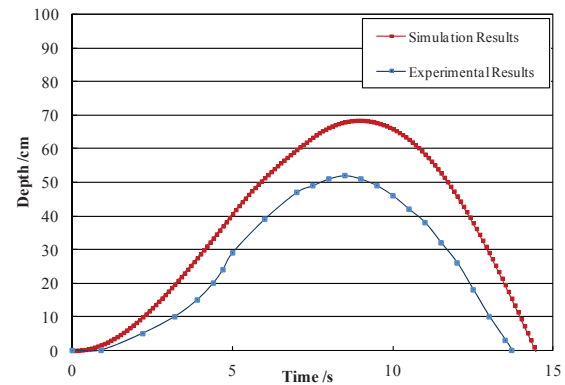
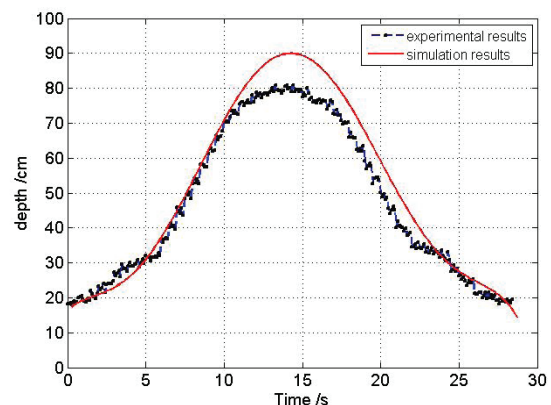


Figure 19 The experiment testing vertical motion with the improved propulsion system



(a) Experimental results for SUR [8]



(b) Experimental results for SUR-II

Figure 20 The experimental results for vertical motion

6. Conclusions

This paper presented a hydrodynamic analysis of the second-generation Spherical Underwater Robot (SUR-II). A static analysis was carried out to improve the rigidity and flexibility of the original design in terms of the structure of the vectored water-jet thruster. The weight of the propulsion system was reduced to 1.08kg. Then, a more efficient propulsion system was developed and mounted on the robot. The robot was described in detail and the three most important degrees of freedom (surge, heave, and yaw) were selected for further analysis. Based on the improved propulsion system, we also carried out a vertical motion experiment to verify the performance of the SUR-II. Comparing the experimental results with our

previous works we found that the improved propulsion system was helpful in enhancing the accuracy of motion.

The related hydrodynamic parameters were estimated before the hydrodynamic analysis to obtain more accurate results. Since the Reynolds number was as high as 1.2×10^5 , the flow was turbulent when the robot was moving. The drag coefficient was estimated for horizontal and vertical motion. Due to the holes in the hull, C_d , when moving horizontally, was as high as 0.61. Then, the maximum velocity in each direction was obtained. All of these parameters were used to establish the appropriate dynamic equation for the robot.

A hydrodynamic analysis was carried out after the main parameter estimation; the robot and water-jet thruster were analysed. For the robot, three main basic motions were analysed to verify the results of the parameter estimation; the drag coefficient converged to 0.41 for the vertical direction and 0.59 for the horizontal direction. These results were very close to the parameter estimation values. The velocity vector and pressure contours clarified the hydrodynamic features and provided important evidence to confirm the assumptions made during the hydrodynamic parameter estimation. Furthermore, the dynamic equation was modified based on the hydrodynamic analysis results. The propulsive force was calculated after post-processing the CFD data. Finally, a propulsive force experiment was used to verify the theoretical and simulation results.

The results of the hydrodynamic parameter estimation and analysis improved the accuracy of the dynamic equations. These results can be used to improve the control accuracy of spherical underwater robots.

7. Acknowledgements

This research was supported by Kagawa University Characteristic Prior Research Fund 2011.

8. References

- [1] S.K. Choi, J. Yuh (1996) Experimental study on a learning control system with bound estimation for underwater robots, *Autonomous Robots. J.* 3(2), 187-194.
- [2] H.T. Choi, A. Hanai, S.K. Choi, J. Yuh (2003) Development of an underwater robot, ODIN-III, *Proceedings of the 2003 IEEE International Conference on Intelligent Robots and Systems*, pp. 836-841.
- [3] S.A. Watson, D.J.P. Crutchley, P.N. Green (2011) The design and technical challenges of a micro-autonomous underwater vehicle AUV, *Proceedings of the 2011 IEEE/ICMA International Conference on Mechatronics and Automation*, pp. 567-572.
- [4] S.A. Watson, P.N. Green (2010) Propulsion Systems for Micro-Autonomous Underwater Vehicles (μ AUVs), *2010 IEEE Conference on Robotics, Automation and Mechatronics*, pp. 435-440.
- [5] S. Guo, J. Du, X. Ye, R. Yan, H. Gao (2011) The computational design of a water jet propulsion spherical underwater vehicle, *Proceedings of the 2011 IEEE International Conference on Mechatronics and Automation*, pp. 2375-2379.
- [6] S. Guo, J. Du, X. Ye, H. Gao, Y. Gu (2010) Realtime adjusting control algorithm for the spherical underwater robot, *INFORMATION-An International Interdisciplinary Journal, J.* 13(6): 2021-2029.
- [7] X. Lan, H. Sun, Q. Jia (2010) Principle and dynamic analysis of a new-type spherical underwater vehicle, *Journal of Beijing University of Posts and Telecommunications J.* 33(3): 20-23 (Chinese)
- [8] X. Lin, S. Guo (2012) Development of a spherical underwater robot equipped with multiple vectored water-jet-based thrusters, *Journal of Intelligent and Robotic Systems. J.* pp. 1-15.
- [9] S. Guo, J. Du, X. Ye, R. Yan, H. Gao (2011) The computational design of a water jet propulsion spherical underwater vehicle, *Proceedings of the 2011 IEEE International Conference on Mechatronics and Automation*, pp. 2375-2379.
- [10] S. Guo, X. Lin, K. Tanaka, Hata, S. (2010) Development and control of a vectored water-jet-based spherical underwater vehicle, *Proceedings of the 2011 IEEE/ICIA International Conference on Information and Automation*, pp. 1341-1346.
- [11] X. Lin, S. Guo, K. Tanaka, S. Hata (2011) Underwater experiments of a water-jet-based spherical underwater robot, *Proceedings of the 2011 IEEE/ICMA International Conference on Mechatronics and Automation*, pp. 738-742.
- [12] M. Ueno, Y. Tsukada, H. Sawada (2011) A prototype of submersible surface ship and its hydrodynamic characteristics, *Ocean Engineering. J.* 38: 1686-1695.
- [13] A. Leroyer, J. Wackers, P. Queutey, E. Guilmineau (2011) Numerical strategies to speed up CFD computations with free surface—Application to the dynamic equilibrium of hulls, *Ocean Engineering. J.* 38: 2070-2076.
- [14] D. Mylonas, P. Sayer (2012) The hydrodynamic flow around a yacht keel based on LES and DES, *Ocean Engineering. J.* 46: 18-32.
- [15] Y. Wei, Y. Wang, S. Chang, J. Fu (2012) Numerical prediction of propeller excited acoustic response of submarine structure based on CFD, FEM and BEM, *Journal of Hydrodynamic. J.* 24(2):207-216.
- [16] H. Cheng, Y. Chien, C. Hsin, K. Chang, P. Chen (2010) A numerical comparison of end-plate effect propellers and conventional propellers, *Journal of Hydrodynamic. J.* 22(5) : 495-500.

- [17] B. Ji, X. Luo, X. Peng, Y. Wu, H. Xu (2012) Numerical analysis of cavitation evolution and excited pressure fluctuation around a propeller in non-uniform wake, *International Journal of Multiphase Flow*. J. 43:13-21.
- [18] X. Lin, S. Guo, K. Tanaka, S. Hata (2010) Development and evaluation of a vectored water-jet-based spherical underwater vehicle, *Information. J.* 13(6): 1985-1998.
- [19] X. Lin, S. Guo, K. Tanaka, S. Hata (2011) Development of a spherical underwater robot, *Proceedings of the 2011 IEEE/ICME International Conference on Complex Medical Engineering*. pp: 662-665.
- [20] C. Yue, S. Guo, X. Lin, J. Du (2012) Analysis and improvement of the water-jet propulsion system of a spherical underwater robot, *Proceedings of the 2012 IEEE/ICMA International Conference on Mechatronics and Automation*, pp.2208-2213.
- [21] X. Jiang, S. Feng, L. Wang (2000) *Underwater robot*. M. Shenyang: Liaoning Science and Technology Publishing House
- [22] E.L. Houghton and P.W. Carpenter (2003) *Aerodynamics for Engineering Students Fifth Edition*, Published by Butterworth-Heinemann, pp. 8-15
- [23] K. Ceylan, A. Altunbas, G. Kelbaliyez (2001) A new model for estimation of drag force in the flow of Newtonian fluids around rigid or deformable particles, *Powder Technology. J.* 119: 250-256
- [24] Kundu, Pijush K., Cohen, Ira M., *Fluid Mechanics*(4th revised ed.), Academic Press, 2009, pp.421-472